Wave-number restriction and mode interaction in Taylor vortex flow: Appearance of a short-wavelength instability

Hans-Georg Paap
Physikalisches Institut der Universität Bayreuth, D-8580 Bayreuth, Federal Republic of Germany

Hermann Riecke
Physikalisches Institut der Universität Bayreuth, D-8580 Bayreuth, Federal Republic of Germany and Institute for Nonlinear Science, University of California, San Diego, La Jolla, California 92093
(Received 5 August 1988; revised manuscript received 17 October 1989)

In the stability analysis of wide-gap axisymmetric Taylor vortex flow, a new instability is found to supersede the Eckhaus instability for sufficiently high Reynolds numbers. Like the Eckhaus instability it is axisymmetric, but it represents a short-wavelength rather than a long-wavelength modulation of the pattern: It tends to eliminate every other vortex pair. In experiments it is therefore expected to change the wave number of the periodic solution more efficiently than the Eckhaus instability. Its origin is traced back to the resonant interaction of modes with wave numbers q and $2q$. The essential features of the bifurcation diagrams connected with this mode interaction can be obtained by considering a degenerate codimension-2 bifurcation.

I. INTRODUCTION

Pattern selection is a problem that appears quite generally in pattern-forming systems such as Rayleigh-Bénard convection,[1] Taylor vortex flow, and directional solidification.[2] For quasi-one-dimensional patterns such as roll convection, this involves in particular the question of the width of the band of stable wave numbers. Close to threshold this band is—for stationary patterns—limited by the universal Eckhaus instability, which involves a one-dimensional modulation of the pattern on a very long length scale. This instability can, however, be superseded by higher-dimensional instabilities; for example, cross rolls or the oscillatory instability in Rayleigh-Bénard convection or wavy vortices in Taylor vortex flow. The question arises whether in these systems the Eckhaus instability is the only quasi-one-dimensional instability restricting the wave-number band and, in particular, whether there is also a quasi-one-dimensional short-wavelength instability.

Close to threshold stationary patterns are described by an amplitude equation with real coefficients. In the one-dimensional case this equation exhibits only the Eckhaus instability. Therefore, to address the question of the existence of a short-wavelength instability one has to go further into the nonlinear regime and choose a system that allows one to exclude higher-dimensional instabilities. This is made possible for Taylor vortex flow by taking a system with a radius ratio $\eta=R_2/R_1$ well below 1. In addition, the Taylor system offers the possibility of precise measurements of the stability boundaries,[3] as shown in previous experimental[4] and theoretical[5] investigations for the radius ratio $\eta=0.75$. In these studies it has been found that already rather close to threshold the band found experimentally deviates substantially from that given by the Eckhaus instability, as determined by amplitude expansions around the critical Reynolds number $\mathcal{R}_c$. In contrast to some expectations it has turned out that this is not due to the appearance of another instability, which according to the experimental observations also would have had to be axisymmetric. Instead, already very close to threshold, $\epsilon_R=(\mathcal{R}-\mathcal{R}_c)/\mathcal{R}_c \simeq 0.15$, the periodic solutions themselves change their character drastically. Their instability, however, is still governed by the same Eckhaus instability even up to $\epsilon_R=1$, where the transition to wavy vortices occurs. To investigate axisymmetric vortices for larger values of ϵ_R, the radius ratio has to be decreased further. This is done in the present work. It is shown that in fact, for $\eta=0.5$, which shifts the onset for wavy vortices to values above $\epsilon_R=3$,[6] one finds a transition to a short-wavelength instability which, instead of modulating the vortices over a long length scale, tends to pair adjacent vortices.

The organization of the paper is as follows. In Sec. II the results of the numerical linear stability analysis of axisymmetric Taylor vortex flow are discussed. These results have been presented previously.[7,8] In Sec. III it is shown that the new instability found in Sec. II is connected with the bifurcations that arise from the interaction of modes with resonating wave numbers. In Sec. IV a bifurcation analysis is performed which captures all qualitative features of the numerically obtained bifurcation diagrams.

II. STABILITY ANALYSIS

Here we investigate the stability of axisymmetric Taylor vortex flow with respect to general axisymmetric disturbances. In order to be able to go to large Reynolds numbers a small radius ratio of $\eta=0.5$ is used throughout this paper. The basic equations as well as the notation are the same as in Ref. 5, which hereafter will be

referred to as RP. Thus we use the dimensionless variables $\bar{t}=2\nu t/d^2$, $x=zq/d$ and $\bar{v}=v/\Omega_1 R_1$ for time, axial coordinate, and velocity, respectively. Here d denotes the gap width R_2-R_1, ν the kinematic viscosity, q the dimensionless wave number, and Ω_1 the rotation rate of the inner cylinder. The torque G exerted on the cylinders is made dimensionless via

$$\bar{G}=2\pi R_1^3 \nu \rho' \Omega_1 / d \ ,$$

with ρ' denoting the density of the fluid (G corresponds to $G/\bar{G}$ in RP). As in RP both the calculation of the solutions as well as their stability analysis are performed numerically using a Galerkin expansion in axial Fourier modes and in radial Chebyshev modes.

The result of this stability analysis is shown in Fig. 1. There the stability limit is given by the solid line. The dash-dotted line denotes the neutral curve and the dashed line gives the (Eckhaus) stability limit as determined in a third-order amplitude expansion.[9,10] For $q<q_c$ ($q_c\cong 3.16$) the limit is always given by the Eckhaus instability and as in RP the strong deviations from the amplitude expansion's result are due to a gap in the existence region of the stationary solutions (see also Sec. III). For $q>q_c$, however, a transition to a short-wavelength instability is found for values of ϵ_R above the horizontal bar across the stability limit. The difference between the two instabilities manifests itself in the behavior of the growth rates of the perturbations, which we now discuss.

The linear stability analysis of the (nonlinear) periodic pattern leads to differential equations with coefficients which are periodic in the axial direction. Any axisymmetric perturbation can therefore be written in Floquet form $u_p(qx)\exp(ipqx)$ where u_p is 2π periodic and p is the normalized Floquet exponent. These perturbations imply a modulation of the pattern over a length $L=2\pi/pq$. This is illustrated in Fig. 3(a) (below) which shows a periodic pattern (dashed line) and the same pattern with a (Floquet) perturbation added at some amplitude (solid line, $p=0.1$). The analysis gives a dispersion relation for the growth rate $\sigma=\sigma(p)$. This dispersion relation depends on $\mathcal{R}$, q, and also on the radius ratio η. Within the stable band σ is negative for all p. On the stability boundary σ goes through 0 at some value p_u and the character of the instability depends on this value.

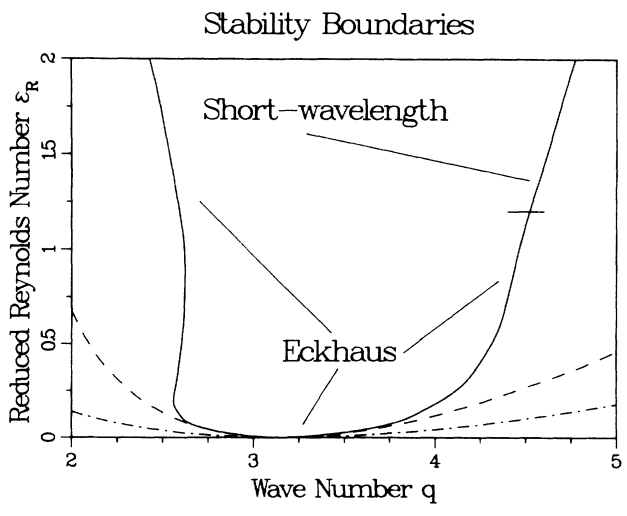

FIG. 1. Stability boundaries for $\eta=0.5$. ——, full stability anslysis; — — —, third-order amplitude exapnsion; —·—·—·, neutral curve. The horizontal bar indicates the transition region between Eckhaus and short-wavelength instability.

The Eckhaus instability is characterized by $p_u\to 0$. To make this more clear it is useful to expand σ in p. Due to the reflection symmetry in the axial direction σ is quadratic in p and one has

$$\sigma=s_2(\mathcal{R},q)p^2+s_4(\mathcal{R},q)p^4+\cdots \ . \tag{1}$$

The onset of the Eckhaus instability is given by a sign change of s_2. Therefore σ becomes positive first for infinitesimally small values of p and the relevant modulations have an essentially infinite wavelength and can be described by a phase diffusion equation. In fact, the phase diffusion coefficient[11,12] $D_\parallel$ is given by $D_\parallel=-s_2/q^2$. A typical behavior of σ in this regime is shown in Fig. 2(a) where $\sigma(p)$ is given for three different values of q for $\epsilon_R=0.555$. The growth rate $\sigma(p)$ has to be symmetric with respect to $p=0.5$ and periodic in p with period 1, since for $p>1$ prefactors $\exp(iqx)$ can be included in u_p. This implies that for larger p more Fourier modes have to be retained to achieve the same accuracy and deviations from periodicity are the effect of the truncation in the number of Fourier modes. The present results were obtained with up to 15 Fourier modes and 14 Chebyshev modes which lead to full matrices of the order 400×400. Note the positive values of σ for $q=0.555$ for small values of p and also the shift of the maximum of $\sigma(p)$ towards larger values of p with increasing q. Thus further beyond the stability limit the maximal growth rate occurs for $p\cong 0.5$.

For larger ϵ_R the dispersion relation behaves differently. This is shown in Fig. 2(d) for $\epsilon_R=1.54$. Now σ becomes positive first for $p_u=\frac{1}{2}$ rather than $p_u\to 0$ and the relevant perturbations modulate the pattern with a wavelength which is twice the wavelength of the basic pattern. We call this new instability *short-wavelength instability*. Figures 2(b) and 2(c) show $\sigma(p)$ for the transition regime between the Eckhaus and the short-wavelength instability. So far the analysis cannot tell whether the short-wavelength instability leads to a new stable solution with twice the original wavelength or not. In Sec. III it will be shown that the bifurcation is in fact backward. Therefore it is expected that, similar to the Eckhaus instability, the instability will change the wave number of the solution and lead back to the stable band.

Despite the fact that both instabilities are axisymmetric they should be fairly distinguishable in experiments. This is illustrated in Figs. 3(a) and 3(b) where the destabilizing linear modes for $\epsilon_R=1.0$ (Eckhaus with $p=0.1$) and for $\epsilon_R=1.54$ ($p=\frac{1}{2}$) have been added with some amplitude to the corresponding periodic solutions. As expected the Eckhaus mode modulates the solution on a long length scale, which compresses and expands the vortices on that scale (arrows). Due to the wave-number

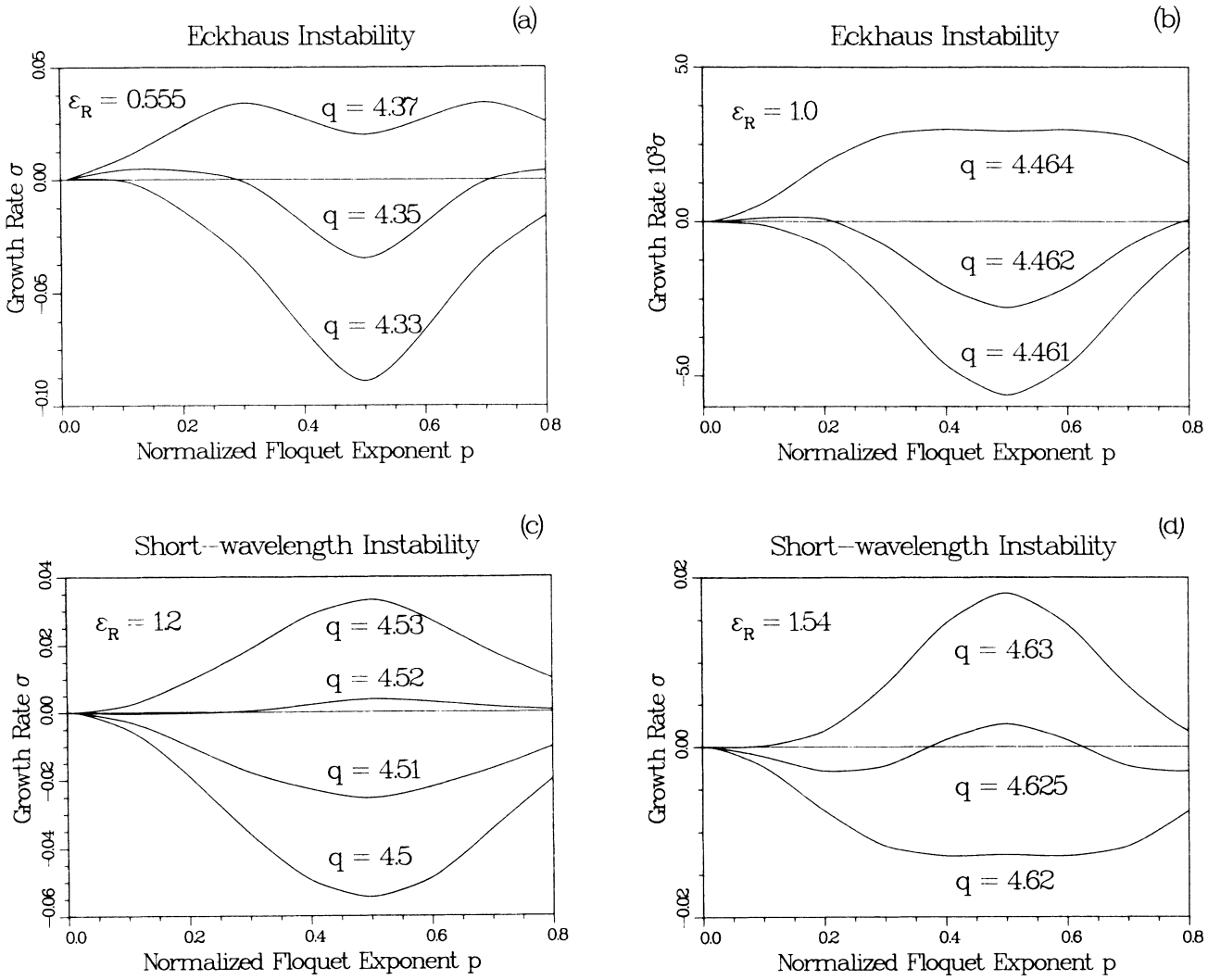

FIG. 2. Growth rate of perturbations as a function of the Floquet exponent. (a) $\epsilon_R = 0.555$, (b) $\epsilon_R = 1.0$, (c) $\epsilon_R = 1.2$, and (d) $\epsilon_R = 1.54$.

dependence of the phase diffusion coefficient the compression (for $q > q_c$) grows without bound and eventually eliminates a vortex pair. For $q < q_c$ the expansion dominates and leads to the creation of a vortex pair. Thus, in the limit $p \to 0$, only a single vortex pair is eliminated (or created) in the whole system. In a long system the wave number therefore changes only slightly. The short-wavelength instability, however, weakens and compresses every second vortex pair and tends to eliminate them (arrows). To describe the destabilizing mode close to the onset of the instability one can derive an amplitude equation[7] which allows also for modulations of this mode on a long length scale. This scale diverges at the instability limit. Close to this limit the destabilizing mode will therefore be extended throughout the whole system and is expected to eliminate half of the vortex pairs. This would reduce the wave number to $q/2$, a wave number for which the pattern again will be unstable for $\epsilon_R < 2$. This instability can therefore be expected to change the wave number quite drastically. In actual experiments (and numerical simulations) one has to take into account that one obtains an approximation of the unstable state starting from a given stable state. Therefore the unstable state is perturbed in a definite way. If this perturbation has a much larger component for small p than close to $p = \frac{1}{2}$ the Eckhaus instability could outrun the short-wavelength instability despite its smaller growth rate. To avoid this one has to cross the stability boundary very slowly so as to obtain a state for which the growth rate is still negative for small p but already positive for $p \cong 0.5$ [compare $q = 4.625$ with $q = 4.63$ in Fig. 2(d)].

III. BIFURCATION DIAGRAMS AND SHORT-WAVELENGTH INSTABILITY

The origin of the short-wavelength instability can be traced back to the same bifurcation structure that leads

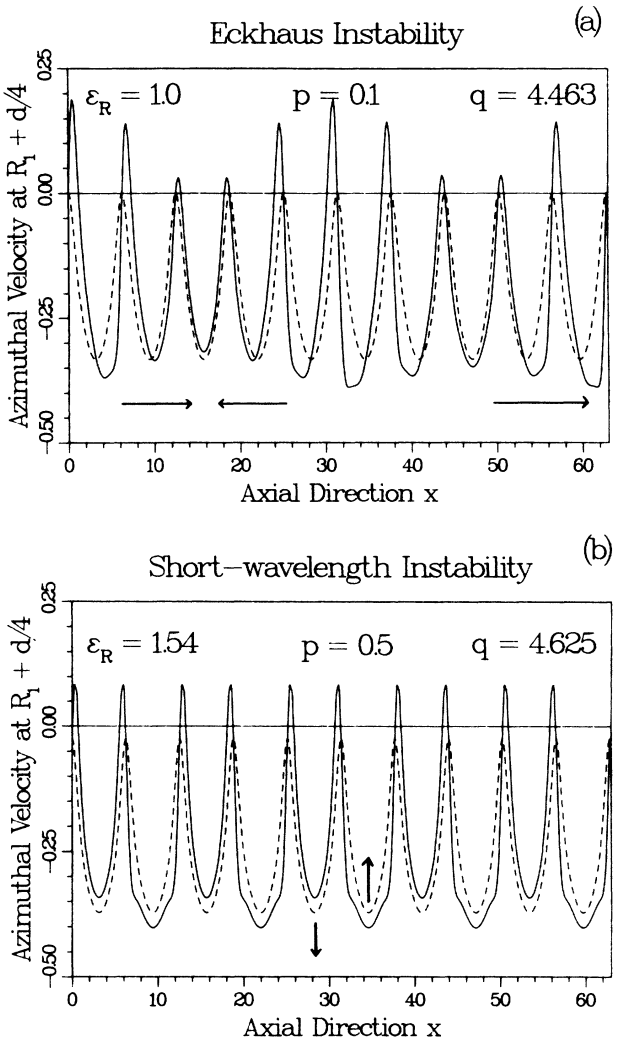

FIG. 3. Destabilizing mode for (a) Eckhaus and (b) short-wavelength instability. — — —, periodic solution; ——, periodic solution with perturbation added at some amplitude. Note that the Eckhaus instability weakens only the middle vortices, whereas the short-wavelength instability tends to eliminate every second pair.

to the strong and sudden deviation from the result of the amplitude expansion for $q < q_c$ and $\epsilon_R \geq 0.15$. As discussed in RP this structure arises from the interaction of modes with resonating wave numbers. The first such resonance occurs for the modes q and $2q$. This has been discussed by various authors, both numerically[13,14,5,15] as well as analytically.[16,17]

To demonstrate that the short-wavelength instability is in fact connected with this resonance and to illustrate the resulting bifurcations in detail, we show a succession of bifurcation diagrams for increasing values of the Reynolds number. We consider a system of length L with periodic boundary conditions. In Figs. 4(a)–4(e) the dimensionless torque exerted on the outer cylinder is exhibited as a function of $2\pi/L$ for the various solutions that exist for given values of ϵ_R and L. We choose the notation $2\pi/L$ rather than q because the figures display also solutions with periodicity length $L/2$ and $L/3$ which have wave numbers $4\pi/L$ and $6\pi/L$. For all Reynolds numbers there exists the Couette flow which is purely azimuthal and yields a torque which is independent of L. At A and C a solution with one pair of Taylor vortices branches off the Couette flow. This solution, which is denoted by S_+, is given by the solid line and has wave number $q = 2\pi/L$. For sufficiently large L, i.e., small $2\pi/L$, an additional solution with two equal vortex pairs (S_2, dashed) becomes possible which is equivalent to a solution at $L/2$ with one vortex pair. Its wave number is therefore twice that of S_+. These are all the solutions possible close to threshold ($\epsilon_R \to 0$). Close to the codimension-2 point ($\epsilon_{Rc_l} = 0.087$, $q_{c_l} = 2.2$), however, where the solution with two vortex pairs branches off the Couette flow simultaneously with that with one pair, additional solutions appear. This was first shown by Andreichikov[13] and is demonstrated in Fig. 4(a); already below ϵ_{Rc_l} a mixed mode solution (S_-, solid) branches off S_2 and merges with it again. This solution consists of two vortex pairs of different sizes. For all Reynolds numbers it bifurcates off S_2 defining bifurcation point $\bar{B}$. Depending on the Reynolds number, however, it merges with different solutions. For $\epsilon_R = 0.0808$ [Fig. 4(a)] this is S_2, whereas for $\epsilon_R = 0.0927$ [Fig. 4(b)] it is the Couette flow (at C). In addition, the bifurcation at $\bar{B}$ has turned backward yielding a saddle-node bifurcation on this branch. Now S_+ does not branch off the Couette flow any more for large L; instead, it merges with S_2 in a forward bifurcation at B. This shows that S_+ should, in fact, also be considered a mixed mode solution since its second harmonic, which is of course present for all L, becomes stronger with growing L and eventually is dominant close to B. Increasing ϵ_R [Fig. 4(c)] turns the bifurcation at C from backward to forward and that at B from forward to backward creating a saddle-node bifurcation at F. Note that for lengths L between F and $\bar{B}$ there exists no nonlinear time-independent solution with only one vortex pair. This is true despite the fact that Couette flow is unstable also with respect to such perturbation. For $\epsilon_R = 0.27$ [Fig. 4(d)] S_- does not reach the Couette flow any more; instead, it merges with an additional solution which has three equal vortex pairs (dash-dotted line). Finally, for $\epsilon_R = 1.54$ [Fig. 4(e)] S_- exhibits a new saddle-node bifurcation and the bifurcation at B becomes very strongly backward.

To see whether this bifurcation structure is at all relevant for the experimental *extended* system and its stability boundaries as given in Fig. 1 one has to compare the Eckhaus stability limits of S_+ with the bifurcation points B and $\bar{B}$. This shows that for small ϵ_R the bifurcation points are far out in the Eckhaus-unstable region [Fig. 4(d)] and therefore rather unimportant. However, with increasing ϵ_R the Eckhaus limit approaches $\bar{B}$ and above $\epsilon_R = 1.2$ the solution is Eckhaus stable all the way to $\bar{B}$ [Fig. 4(e)]. Therefore the short-wavelength instability can be identified as the bifurcation of S_- off S_2 at $\bar{B}$, since the latter solution is equivalent with S_+ far away from the codimension-2 point. In addition, this shows

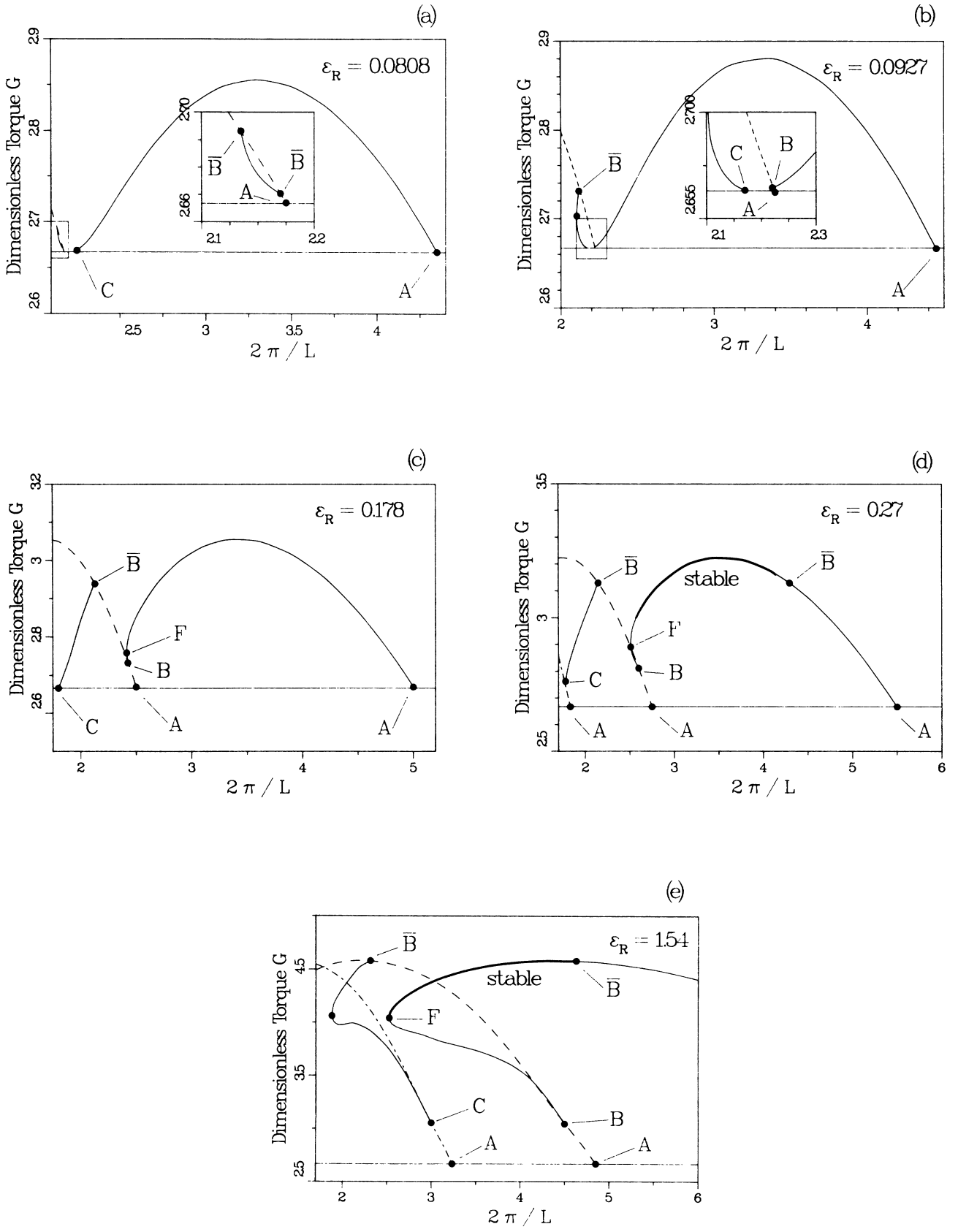

FIG. 4. Dependence of the bifurcation diagram on the Reynolds number. The heavy line indicates the region of stable axisymmetric vortices. When this region reaches $\bar{B}$ the Eckhaus instability is superseded by the short-wavelength instability. For details see text.

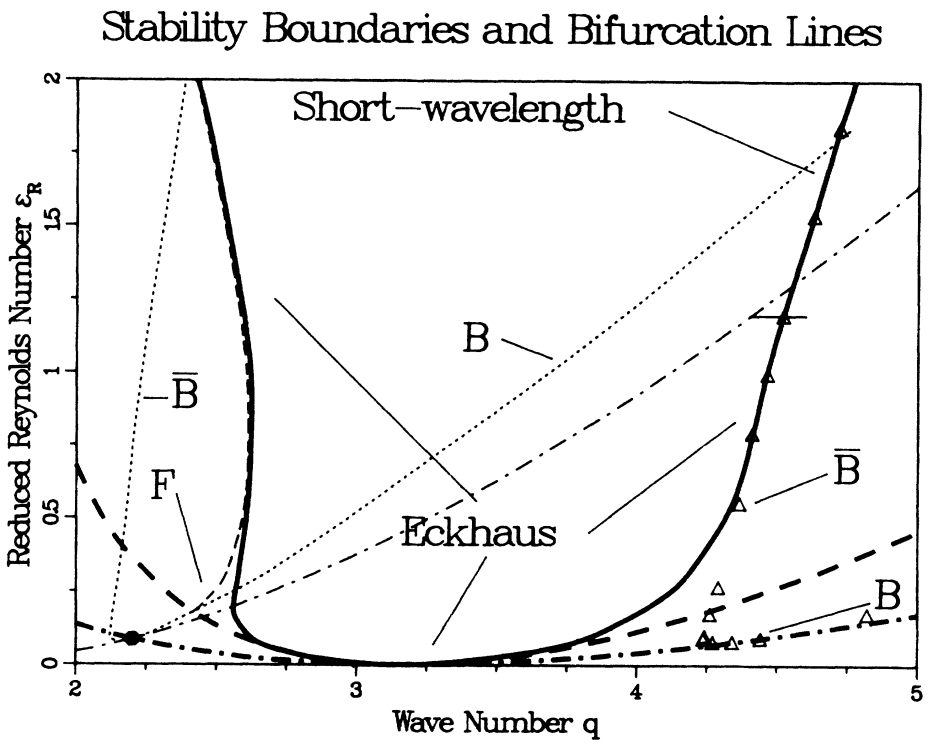

FIG. 5. Location of the bifurcations B, $\bar{B}$, and F with respect to the stability boundaries. Heavy lines as in Fig. 1. —·—·—·, neutral curve for S_2 (A in Fig. 4); · · · ·, B and $\bar{B}$ (for large q the same curve is shown by Δ to distinguish it from the stability boundary); — — —, saddle-node bifurcation of S_+ at F. The codimension-2 point (●) is given by the intersection of the two neutral curves.

that in the present case there is no additional stable periodic solution beyond the stability limit. As indicated above the short-wavelength instability is therefore expected to lead back to the stable band.[18,19]

These bifurcation diagrams are summarized in Fig. 5 where the locations of the bifurcations at B and $\bar{B}$ (dotted lines) as well as that of the saddle-node bifurcation at F (short dashes) are given together with the stability limits. The codimension-2 point is given by the intersection of the neutral curve for modes with one vortex pair per length L (thick dash-dotted line) and that for modes with two vortex pairs (thin dash-dotted lines). The triangles give the location of B and $\bar{B}$ when they are interpreted as bifurcations off S_+ rather than S_2. $\bar{B}$ gives the onset of the short-wavelength instability. Below $\epsilon_R \cong 1.2$ (horizontal bar) it is superseded by the Eckhaus instability (thick line), whereas above $\epsilon_R \cong 1.2$ it occurs just before the Eckhaus instability [cf. Fig. 2(d)]. Figure 6 shows an enlargement of Fig. 5 in the vicinity of the codimension-2 point with the saddle-node line of S_- added. The arrows show the range of existence for the respective solutions. Close to the saddle-node lines the arrows turn around to indicate the existence of two such solutions.

IV. BIFURCATION ANALYSIS

In the following we discuss how most of the qualitative features of the bifurcation diagrams shown in Fig. 4 can be understood through a bifurcation analysis of the interaction of two modes with resonating wave numbers. This extends the analysis of Dangelmayr[16] to a degenerate case which has been considered to some extent by Busse[20] for weakly non-Boussinesq Rayleigh-Bénard convection.

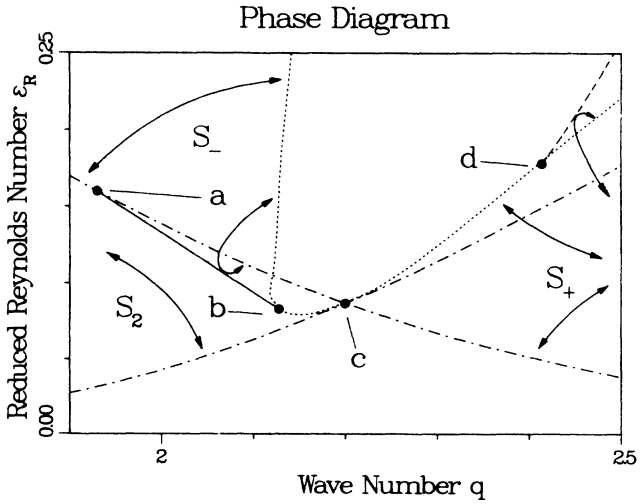

FIG. 6. Phase diagram close to the codimension-2 point. —·—·—·, neutral curves for S_2 and S_+ (A in Fig. 4); · · · ·, B and $\bar{B}$; — — —, saddle-node bifurcation of S_+ at F; ——, saddle-node bifurcation of S_-.

We consider Taylor vortex flow close to the point in parameter space where both a mode with wave number q as well as one with wave number $2q$ bifurcate from the basic state simultaneously. In the vicinity of this (codimension-2) point the dynamics of the system can be reduced to that on the center manifold spanned by these two unstable modes,[21] and the flow field is given by

$$\mathbf{v}(r,z)=\zeta_1 e^{iqx}\boldsymbol{\phi}_1(r)+\zeta_2 e^{2iqz}\boldsymbol{\phi}_2(r)+\text{c.c.}+\cdots , \quad (2)$$

with $\boldsymbol{\phi}_i(r)$ being the linear eigenvectors corresponding to the mode with wave number q and $2q$, respectively, and the ellipsis representing higher-order terms. This yields two ordinary differential equations for the complex amplitudes ζ_1 and ζ_2. As in the numerical calculation we assume periodic boundary conditions. Therefore the amplitude equations have to be invariant under translations $T_d: z\to z+d$ and reflections $K: z\to -z$. These symmetries transform the amplitudes ζ_1 and ζ_2 according to

$$T_d(\zeta_1,\zeta_2)=(e^{iqd}\zeta_1, e^{2iqd}\zeta_2), \quad K(\zeta_1,\zeta_2)=(\zeta_1^*,\zeta_2^*) . \quad (3)$$

As shown by Dangelmayr[16] this leads to the amplitude equations

$$\begin{aligned}\partial_t\zeta_1&=(\alpha+a_1|\zeta_1|^2+b_1|\zeta_2|^2)\zeta_1+c_1\zeta_2\zeta_1^* ,\\ \partial_t\zeta_2&=(\beta+a_2|\zeta_1|^2+b_2|\zeta_2|^2)\zeta_2+c_2\zeta_1^2 .\end{aligned} \quad (4)$$

The coefficients a_i, b_i, and c_i as well as α and β are real. The small parameters α and β are the unfolding parameters and are related to ϵ_R and q via

$$\begin{aligned}\alpha&=\lambda(\epsilon_R-\epsilon_{Rct})+\kappa(q-q_{ct})+\cdots ,\\ \beta&=\lambda'(\epsilon_R-\epsilon_{Rct})-\kappa'(q-q_{ct})+\cdots ,\end{aligned} \quad (5)$$

with λ, λ', κ, and κ' being positive quantities of order 1. The neutral curves for the modes ζ_1 and ζ_2 are given by $\alpha=0$ and $\beta=0$, respectively. It is not our aim here to calculate the coefficients λ, λ', κ, κ', a_i, b_i, and c_i quantitatively. Instead, we ask whether these equations allow qualitatively the same bifurcation scenario as that found in the numerical calculation.

Assuming c_1 and c_2 to be nonzero, Dangelmayr performs a nonlinear coordinate change which simplifies these amplitude equations to the corresponding normal form.[16] The resulting equations describe the bifurcations in Taylor vortex flow correctly very close to the codimension-2 point including the subcritical bifurcation of S_- between $\bar{B}$ and $\bar{\bar{B}}$ [see Fig. 4(a)]. However, the saddle-node bifurcations of S_+ [see Fig. 4(c)] and S_- [see Fig. 4(b)] cannot be obtained. As will be shown below, this is achieved if one considers the degenerate bifurcation where c_1 and c_2 are small and taken as additional unfolding parameters. Note that for $c_1=c_2=0$ the system has an additional reflection symmetry $\zeta_{1,2}\to-\zeta_{1,2}$. This sign change of the velocity field corresponds to an interchange of inflow and outflow, which is a symmetry of Taylor vortex flow only in the limit $\eta\to 1$ and corotating cylinders ($\mu\to 1$). Thus by taking c_1 and c_2 as (small) unfolding parameters, we are considering Taylor vortex flow close to that limit. It turns out, however, that the qualitative features of the phase diagram are the same as in the wide-gap system calculated numerically in Sec. III. Therefore this degenerate codimension-2 bifurcation can be regarded as an "organizing center" for Taylor vortex flow which captures the bifurcation scenario over a wide range of radius ratio and Reynolds number.

In the general case (allowing c_1 and c_2 also to be small) no additional coordinate transformation is possible. Introducing $\zeta_1=Ae^{i\varphi}$ and $\zeta_2=Be^{i\rho}$ the amplitude equations read in the static case

$$\begin{aligned}&(\alpha+a_1A^2+b_1B^2+c_1B)A=0 ,\\ &(\beta+a_2A^2+b_2B^2)B+c_2A^2=0 .\end{aligned} \quad (6)$$

The first equation yields either $A=0$ or

$$A^2=-(\alpha+b_1B^2+c_1B)/a_1 , \quad (7)$$

which gives an equation for B,

$$-c_2\alpha+(a_1\beta-a_2\alpha-c_1c_2)B-(c_1a_2+c_2b_1)B^2+(a_1b_2-a_2b_1)B^3=0 . \quad (8)$$

The qualitative features we want to obtain are the saddle-node bifurcations of S_+ and S_- [see Figs. 4(b) and 4(c)]. To this end it is sufficient to show that the bifurcation of S_- from the Couette flow ($A=0$, $B=0$) at C as well as that of S_- (at $\bar{B}$) and S_+ (at B) from S_2 change from backward to forward (or vice versa). In Fig. 6 these locations are indicated by points a, b, and d, respectively.[22]

At the saddle node there exist two real solutions to Eqs. (7) and (8). At point a this saddle node occurs at the neutral curve, which implies that Eq. (8) has a double zero $B=0$ (and $A=0$). This yields

$$\begin{aligned}\alpha_a&=0 ,\\ \beta_a&=c_1c_2/a_1 .\end{aligned} \quad (9)$$

Equation (9) clearly shows that this point can only be obtained in such a bifurcation analysis in the degenerate case where c_1c_2 is small.

At points b and d, S_+ and S_- bifurcate, respectively, tricritically off S_2. This solution is given by

$$A=0, \quad B_0^2=-\beta/b_2 , \quad (10)$$

and the bifurcation line is given by

$$0=\alpha+b_1B_0^2+c_1B_0 . \quad (11)$$

The points b and d therefore satisfy Eqs. (10) and (11) combined with the condition for a double zero of (8),

$$a_1\beta_0-a_2\alpha_0-c_1c_2-2B_0(c_1a_2+c_2b_1)+3B_0^2(a_1b_2-a_2b_1)=0 . \quad (12)$$

Using (10) and (11) α and β can be eliminated from (12) yielding

$$2(a_1b_2-a_2b_1)B_0^2-(a_2c_1+2c_2b_1)B_0-c_1c_2=0 \quad \text{if } B_0>0 , \quad (13a)$$

$$2(a_1b_2-a_2b_1)B_0^2-(3a_2c_1+2c_2b_1)B_0-c_1c_2=0 \quad \text{if } B_0<0 . \tag{13b}$$

If $a_1b_2-a_2b_1$ and c_1c_2 have the same sign the two roots $B_0^{(1,2)}$ of (13a) [as well as those of (13b)] have opposite signs. Thus one tricritical point occurs with $B_0>0$ [from (13a)] and one with $B_0<0$ [from 13(b)]. This corresponds to the result found in Sec. III where both branches S_+ and S_- exhibit a tricritical point. In the general case (13) can have more than two solutions. This is related to the fact that as a function of α (or β) Eq. (8) can have up to three saddle nodes since its discriminant is a cubic polynomial in α (and β). Also, two saddle nodes can occur on the same branch. A complete classification of the possible bifurcations is complicated by the fact that physically acceptable solutions have to satisfy in addition $A^2>0$ [cf. Eq. (7)]. Some more details are given in Ref. 23. Suffice it here to state that for

$$a_1<0 , \tag{14a}$$

$$b_2<0 , \tag{14b}$$

$$c_1c_2<0 , \tag{14c}$$

$$a_2b_1>a_1b_2 , \tag{14d}$$

the scenario of Sec. III can be reproduced, provided $A^2>0$ at two saddle nodes: S_- and S_2 bifurcate from Couette flow supercritically (S_- only for $\beta>\beta_a$), point a lies above the neutral curve for S_2, and both b and d exist. Suitable values of the coefficients are, for instance,[23] $a_1=b_1=-1.5$, $c_1=-0.15$, $a_2=-8$, $b_2=-2$, and $c_2=0.81$. Thus, after relaxing the nondegeneracy condition $c_1c_2\neq 0$, this bifurcation analysis can capture the observed behavior of wide-gap Taylor vortex flow over a considerably larger range of Reynolds number. This analysis applies also to directional solidification where similar bifurcation diagrams are observed.[2]

V. CONCLUSION

In conclusion, it has been shown that in axisymmetric Taylor vortex flow the Eckhaus instability is superseded by another axisymmetric instability if the Reynolds number is increased beyond twice the critical value. This new instability modulates the solution at half the wave number and is expected to change the number of vortices in the system drastically. It originates from the interaction of resonating modes. All qualitative features of the observed bifurcation diagrams can be understood by an analytical bifurcation analysis of this mode interaction if one expands in the asymmetry between inflow and outflow. Considering also the results of RP it is seen that these resonating modes profoundly influence the limits of the experimentally observable band width for both $q<q_c$ as well as $q>q_c$. It is interesting to note that for sufficiently large Reynolds numbers the bifurcation analysis of *strictly periodic* solutions gives a rather good account of the stable wave-number band of the extended system, which also allows *slow spatial modulations.* This is due to the fact that for $q<q_c$ the Eckhaus instability occurs only very close to the saddle node and for $q>q_c$ it is replaced by the short-wavelength instability. Similar results may also be expected in directional solidification[2] and other quasi-one-dimensional systems which break the reflection symmetry $\zeta\rightarrow-\zeta$.[24]

ACKNOWLEDGMENTS

We gratefully acknowledge discussions with L. Kramer, F. H. Busse, J. D. Crawford, H. Levine, and D. S. Cannell and wish to thank the computer center of the Universität Karlsruhe for providing free computer time. H.R. also acknowledges support by U.S. Air Force Grant No. AFOSR F49620-87-C-0117 and the Deutsche Forschungsgemeinschaft.

[1]C. Normand, Y. Pomeau, and M. G. Velarde, Rev. Mod. Phys. **49**, 581 (1977).
[2]D. A. Kessler and H. Levine, Phys. Rev. A **39**, 3041 (1989).
[3]G. Ahlers, D. S. Cannell, and M. A. Dominguez-Lerma, Phys. Rev. A **27**, 1225 (1983).
[4]M. A. Dominguez-Lerma, D. Cannell, and G. Ahlers, Phys. Rev. A **34**, 4956 (1986).
[5]H. Riecke and H.-G. Paap, Phys. Rev. A **33**, 547 (1986).
[6]C. A. Jones, J. Fluid Mech. **157**, 135 (1985).
[7]H. Riecke, Ph.D. thesis, Universität Bayreuth, 1986.
[8]H.-G. Paap and H. Riecke, Verh. Dtsch. Phys. Ges. **1**, DY-14.23 (1987).
[9]F. H. Busse, in *Instability of Continuous Systems,* edited by H. Leipholz (Springer, Berlin, 1971).
[10]S. Kogelman and R. C. DiPrima, Phys. Fluids **13**, 1 (1970).
[11]L. Kramer and W. Zimmermann, Physica **16D**, 221 (1985).
[12]H. Riecke and H.-G. Paap, Phys. Rev. Lett. **59**, 2570 (1987).
[13]J. P. Andreichikov, Izv. Akad. Nauk SSSR, Mekh. Zhidk. Gaza **1**, 47 (1977).
[14]R. Meyer-Spasche and H. B. Keller, Phys. Fluids **28**, 1248 (1985).
[15]F. H. Busse and A. C. Or, J. Appl. Math. Phys. (ZAMP) **37**, 608 (1986).
[16]G. Dangelmayr, Dyn. Stab. Syst. **1**, 159 (1986).
[17]C. A. Jones and M. R. E. Proctor, Phys. Lett. A **121**, 224 (1987).
[18]In recent experiments on directional solidification in nematic liquid crystals period-doubled solutions have been found [A. J. Simon, J. Bechhoefer, and A. Libchaber, Phys. Rev. Lett. **61**, 2574 (1988)]. One may speculate that they may be due to the same mode interaction as the short-wavelength instability discussed here, with the bifurcation at $\bar{B}$ being forward instead of backward.
[19]A. J. Simon, J. Bechhoefer, and A. Libchaber, Phys. Rev. Lett. **61**, 2574 (1988).
[20]F. H. Busse in *Bifurcation: Analysis, Algorithms, Applications,*

edited by T. Küpper, R. Seydel, and H. Tröger (Birkhäuser, Basel, 1987).

[21]J. Guckenheimer and P. Holmes, *Nonlinear Oscillations, Dynamics Systems, and Bifurcations of Vector Fields* (Springer, Berlin, 1986).

[22]The mode interaction leads also to bifurcations to traveling and standing waves (Refs. 16 and 17). They are, however, not necessary for an understanding of the short-wavelength instability.

[23]H.-G. Paap, Ph.D. thesis, Universität Bayreuth, 1989.

[24]M. Rabaud, S. Michalland, and Y. Couder (unpublished).